

Cancer immunophenotyping by seven-colour multispectral imaging without tyramide signal amplification

Marieke E Ijsselsteijn^{1†} , Thomas P Brouwer^{1,2†}, Ziena Abdulrahman¹, Eileen Reidy¹, Ana Ramalheiro¹, A Marijne Heeren³, Alexander Vahmeijer², Ekaterina S Jordanova^{1,3} and Noel FCC de Miranda^{1*}

¹Department of Pathology, Leiden University Medical Centre, Leiden, The Netherlands

²Department of Surgery, Leiden University Medical Centre, Leiden, The Netherlands

³Department of Gynaecology, Leiden University Medical Centre, Centre for Gynaecologic Oncology, Amsterdam, The Netherlands

*Correspondence to: Noel FCC de Miranda, Department of Pathology, Leiden University Medical Centre, Albinusdreef 2, 2333 ZA Leiden, The Netherlands. E-mail: n.f.de_miranda@umc.nl

†Contributed equally

Abstract

Checkpoint blockade immunotherapies have revolutionised cancer treatment in the last decade. Nevertheless, these are only beneficial for a small proportion of cancer patients. Important prognosticators for response to immunotherapy are the mutation burden of tumours as well as the quality and quantity of tumour-infiltrating immune cells. High-throughput multiplex immunophenotyping technologies have a central role in deciphering the complexity of anti-tumour immune responses. Current techniques for the immunophenotyping of solid tumours are held back by the lack of spatial context, limitations in the number of targets that can be visualised simultaneously, and/or cumbersome protocols. We developed a tyramide signal amplification-free method for the simultaneous detection of seven cellular targets by immunofluorescence. This method overcomes limitations posed by most widespread techniques and provides a unique tool for extensive phenotyping by multispectral fluorescence microscopy. Furthermore, it can be easily implemented as a high-throughput technology for validation of discovery sets generated by RNA sequencing or mass cytometry and may serve in the future as a complementary diagnostic tool.

Keywords: multispectral immunofluorescence; cancer microenvironment; T-cells; myeloid cells; biomarkers; immune infiltration; immunotherapy

Received 24 May 2018; Revised 3 August 2018; Accepted 31 August 2018

No conflicts of interest were declared.

Introduction

Immunotherapy has emerged as one of the most promising treatments for cancer [1–4]. However, a substantial proportion of patients are not responsive to current immunotherapies and, therefore, the discovery of (immune) biomarkers with predictive clinical value has become a major research avenue in cancer immunology [5–8]. It has long been recognised that the type and density of tumour-infiltrating immune cells is an important prognostic indicator in several cancer types [9–12]. High-throughput and multiplex immunophenotyping technologies are, thus, fundamental for research purposes but also carry great potential for implementation in a diagnostic setting. However, few tools are currently available for extensive immunophenotyping

of tumour tissues in readily available clinical samples (often formalin-fixed, paraffin-embedded [FFPE] tissues).

Singleplex or multiplex immunohistochemistry (IHC) and immunofluorescence (IF) are the gold standard for the analysis of archival tumour tissues, but a major drawback of these techniques is the limited number of targets that can be detected simultaneously. Flow cytometry, on the other hand, has been successfully implemented for diagnostic purposes as well as for monitoring treatment responses [13,14]. However, the lack of tissue-context data generated by flow cytometry remains a limitation for the analysis of solid tumours [15]. Mass cytometry and transcriptomic technologies have demonstrated great value for characterisation of cancer immune landscapes but are better

applicable in a discovery setting and less suitable for high-throughput investigation of biomarkers [16–18]. An emerging tool that can overcome these limitations is sequential IHC of tissue sections with alternating immune detection and bleaching steps. Later, images are digitally overlaid to construct a ‘multiparametric’ image [19,20]. Furthermore, the Opal™ 6-plex quantitative IF assay, in combination with multispectral imaging systems, allows for multiplex IF detection on a single tissue section through sequential steps of tyramide signal amplification (TSA), followed by microwave-mediated antibody stripping [21–23]. Nevertheless, sequential immune detection methods are time-consuming and antibody stripping can compromise tissue integrity and morphology, which limits its application in certain tissue types (e.g. bone or adipose tissue).

We developed a seven-colour IF method for the analysis of FFPE tissues, which can be used for extensive phenotyping by multispectral fluorescence microscopy. This protocol overcomes limitations posed by the previous techniques by using a combination of both indirect and direct fluorescence detection of antibody binding. Furthermore, we demonstrate the flexibility of the system as it is easily combined with the TSA method for the improved detection of low-abundance antigens.

Materials and methods

Tissue material

FFPE blocks from tonsil and colorectal cancer tissues were obtained from the Department of Pathology of

the Leiden University Medical Centre (Leiden, The Netherlands). Mismatch repair (MMR) status was determined as either MMR proficient or deficient by immunohistochemical detection of PMS2 and MSH6 proteins [24]. Patient samples were anonymised and handled according to the medical ethical guidelines described in the Code of Conduct for Proper Secondary Use of Human Tissue of the Dutch Federation of Biomedical Scientific Societies.

Immunohistochemistry

Antibody specificity and optimal conditions for antigen retrieval were assessed by singleplex IHC. FFPE 4-µm tissue sections were deparaffinised with xylene and washed in ethanol, after which endogenous peroxidase was blocked by incubation in a 0.3% hydrogen peroxide/methanol (Merck Millipore, Burlington, MA, USA) solution for 20 min. Heat-induced antigen retrieval was done with either citrate buffer (10 mM, pH 6.0) or Tris–EDTA buffer (10 mM/1 mM, pH 9.0). After cooling, non-specific antibody binding sites were blocked for 30 min with Superblock solution (Thermo Fisher Scientific, Waltham, MA, USA) and incubated overnight with a primary antibody (Table 1). After washing in PBS, 1 h incubation with poly-horseradish peroxidase solution (Immunologic, Duiven, The Netherlands) was performed at room temperature (RT). The slides were developed with the DAB+ chromogen (DAKO, Agilent Technologies, Santa Clara, CA, USA) solution and counterstained with haematoxylin (Thermo Fisher Scientific). Optimal IHC conditions were evaluated by light microscopy.

Table 1. Antibodies included in the T-cell and myeloid panels

Target	Clone	Species	Isotype	Detection	Fluorochrome	Supplier
T-cell panel						
Pan-Cytokeratin	AE1/AE3 and C11	Mouse	IgG1	Direct	Alexa 488	Thermo Fisher Scientific
CD8	4B11	Mouse	IgG2b	Indirect	CF555	Cell Signaling Technology
CD3	D7A6E	Rabbit	IgG	Direct	Alexa 594	Cell Signaling Technology
FOXP3	236A/E7	Mouse	IgG1	Indirect	CF633	Thermo Fisher Scientific
CD45RO	UCHL1	Mouse	IgG2a	Indirect	CF647	Cell Signaling Technology
GZMB	EPR8260	Rabbit	IgG	Indirect	Alexa 680	Abcam
DAPI						
Myeloid panel						
PDL1	SP-142	Rabbit	IgG	Opal	Opal 520	Spring Bioscience
CD11c	EP1347Y	Rabbit	IgG	Direct	Alexa 546	Abcam
HLA-DR	TAL 1B5	Mouse	IgG1	Direct	Alexa 594	Thermo Fisher Scientific
CD163	10D6	Mouse	IgG1	Indirect	CF633	Thermo Fisher Scientific
Pan-Cytokeratin	AE1/AE3 and C11	Mouse	IgG1	Direct	Alexa 647	Novus Biologicals/Biolegend
CD68	D4B9C	Rabbit	IgG	Indirect	Alexa 680	Cell Signaling Technology
DAPI						

Direct and indirect immunofluorescent detection

Seven-target IF detection was performed on 4- μm FFPE tissue sections which were deparaffinised with xylene and washed in ethanol. Heat-induced antigen retrieval in citrate buffer (10 mM, pH 6) was performed and the slides were allowed to cool down to RT. Subsequently, the tissues were blocked with Superblock buffer (Thermo Fisher Scientific) and incubated overnight with all primary antibodies to be detected indirectly (Table 1). After incubation, detection with corresponding fluorescent secondary antibodies (CF dye conjugated secondary antibodies, Sigma–Aldrich, Saint Louis, MO, USA; Alexa Fluor dye conjugated secondary antibodies, Thermo Fisher Scientific) was performed followed by incubation of the tissue with directly conjugated primary antibodies. Directly conjugated antibodies were obtained with the corresponding Alexa Fluor (546, 594) antibody labelling kits (Thermo Fisher Scientific). Furthermore, two pre-conjugated (Alexa Fluor 488 for the T-cell panel and Alexa Fluor 647 for the myeloid panel) anti-keratin monoclonal antibodies that detect different keratins were used simultaneously to enhance the signal detection of epithelial tumour cells. Finally, the tissues were incubated with DAPI (1 μM) as nuclear counterstain and mounted with Prolong[®] Gold Antifade Reagent (Cell Signaling Technology, Danvers, MA, USA).

TSA in combination with direct and indirect immunofluorescent detection

For the detection of low abundance proteins, TSA signal amplification was performed with the Opal 7-colour manual IHC kit (Perkin Elmer, Waltham, MA, USA). Deparaffinisation, blocking of endogenous peroxidase, and antigen retrieval in citrate buffer were performed as described previously. Slides were incubated for 1 h with anti-PD-L1 (Clone SP142, Spring Bioscience, Pleasanton, CA, USA) followed by a 30 min incubation with poly-horseradish peroxidase solution (Immunologic). Fluorescence detection was achieved by using the Opal 520 reagent (Perkin Elmer). Finally, after microwave-mediated antibody stripping, the slides were sequentially incubated with primary antibodies, secondary fluorescent antibodies, and directly conjugated antibodies (Table 1), using the previously described method.

Image acquisition and analysis

Tissue slides were imaged at $\times 40$ magnification with the Vectra 3.0 Automated Quantitative Pathology Imaging System (Perkin Elmer). Image analysis and

spectral separation of dyes was performed with the InForm Cell Analysis software (Perkin Elmer) by using spectral libraries defined with single-marker IF detection. To ensure the signals of the single markers were specific, the immunofluorescent detection was compared to chromogenic IHC. Tissue segmentation

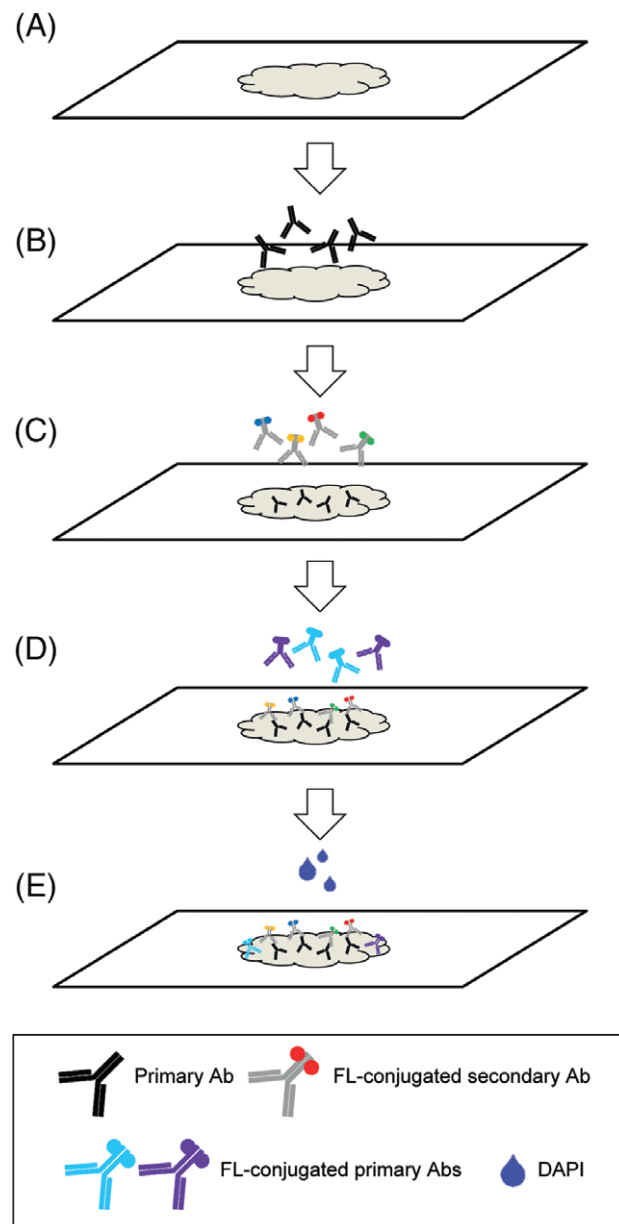


Figure 1. Workflow of seven-target IF detection starting with tissue preparation (A), followed by detection with primary antibodies (B), which are subsequently detected with secondary antibodies (C). Afterwards, the tissue is incubated with directly conjugated antibodies (D), and incubated with DAPI as nuclear counterstain (E).

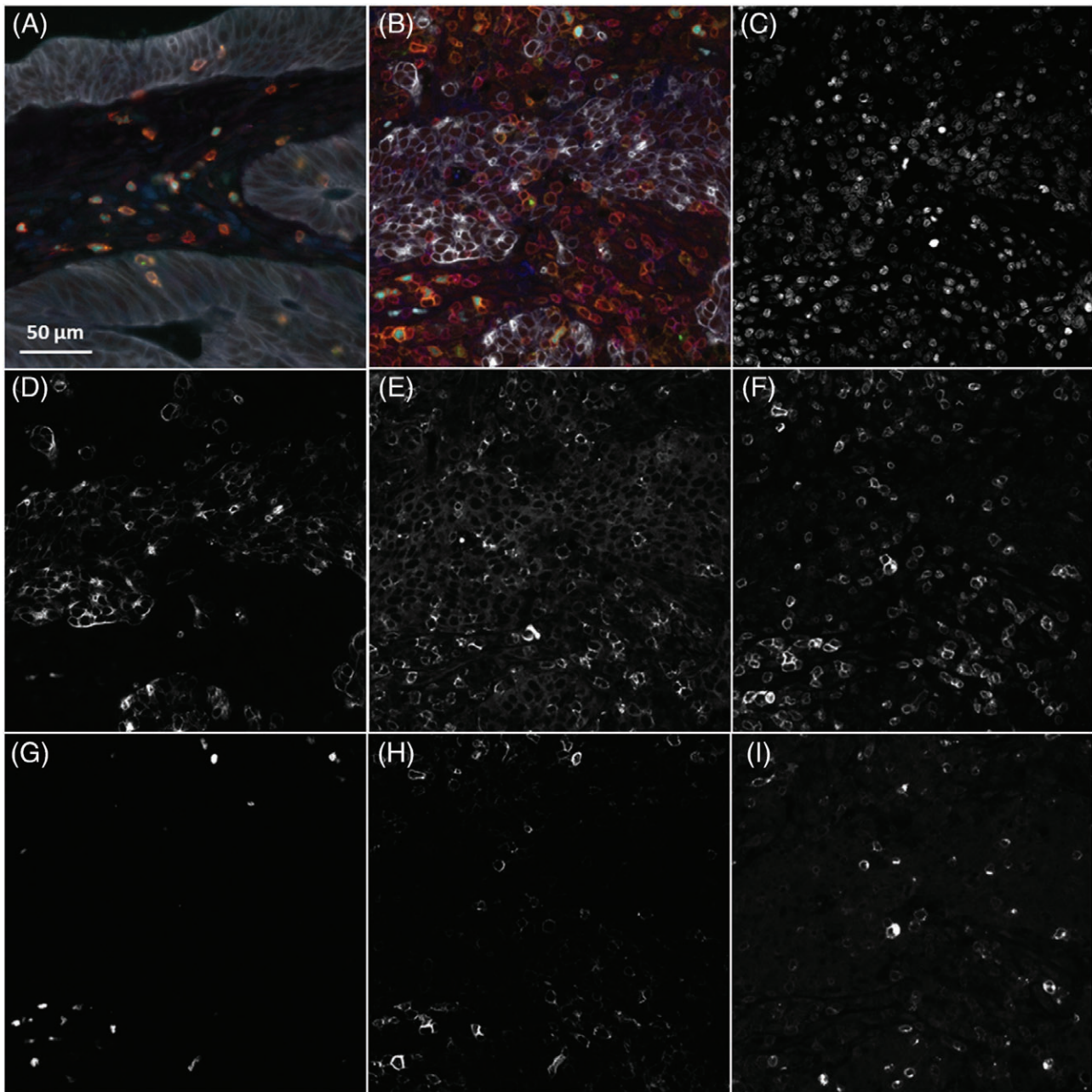


Figure 2. Immunofluorescent detection of T-cell markers in MMR-proficient (A) and MMR-deficient (B) colorectal cancer tissues, namely CD3 (red), CD8 (blue), FOXP3 (cyan), CD45RO (orange), GZMB (green), keratin (white) to distinguish tumour tissue, and DAPI (grey) as nuclear counterstain. Panels C–I show DAPI, keratin, CD8, CD3, FOXP3, CD45RO, and GZMB, respectively, detected in the MMR-deficient tumour presented in panel B.

was trained manually with DAPI and keratin to segment images into tumour, stroma, and ‘no tissue’ areas. Next, cellular segmentation was performed using a counterstain-based approach with DAPI to segment nuclei and membrane markers (CD8, CD3, and CD45RO for the T-cell panel and HLA-DR, CD163, and CD68 for the myeloid panel) to detect cell

contours. Phenotyping was trained manually per tumour where 20 cells per phenotype were defined (Supplementary material, Figure S1). The following phenotypes were identified for the T-cell panel: total T-cells (CD3⁺), CD8⁻ T-cells (CD3⁺CD8⁻, mostly T-helper cells), cytotoxic T-cells (CD3⁺CD8⁺), regulatory T-cells (CD3⁺FOXP3⁺), memory T-cells

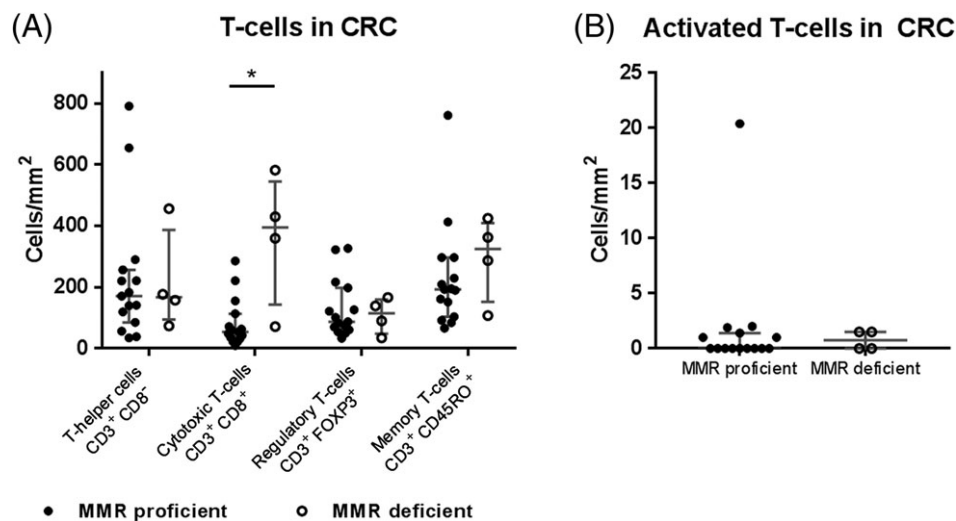


Figure 3. Prevalence of T-cell immunophenotypes in colorectal cancer (CRC) tissue. Phenotypes are defined as T-helper cells ($CD3^+CD8^-$), cytotoxic T-cells ($CD3^+CD8^+$), regulatory T-cells ($CD3^+FOXP3^+$), memory T-cells ($CD3^+CD45RO^+$), and activated T-cells ($CD3^+GZMB^+$).

($CD3^+CD45RO^+$), and activated, cytotoxic T-cells ($CD3^+GZMB^+$). All images were visually inspected to confirm the correct attribution and quantification of phenotypes. For each case, cell counts were normalised by tissue area (number of cells/ mm^2).

Results

The combination of indirect and direct IF detection allows for the simultaneous assessment of seven markers

To assess seven markers in a single tissue slide, a method was developed in which four targets were detected with primary antibodies and isotype/species-specific secondary fluorescent antibodies (Figure 1A–C) followed by the detection of two additional cellular markers with directly conjugated antibodies in order to overcome limitations posed by species/isotype overlap (Figure 1D). Finally, nuclear counterstain was obtained with DAPI (Figure 1E). As a proof of principle, tumour tissues were evaluated for the expression of CD3 and pan-keratin with directly conjugated antibodies while the expression of CD8, FOXP3, CD45RO, and Granzyme B was assessed by indirect IF (Figure 2). After the development of a spectral library with single IF assays, multiplexed images were obtained with the following filter-dye combinations: DAPI, FITC/AF488 (keratin), Cy3/TRITC ($CD8$ -CF555), Texas Red ($CD3$ -AF594), and Cy5 ($FOXP3$ -CF633, $CD45RO$ -CF647, $GZMB$ -AF680).

Importantly, antibodies were titrated so that spectral overlap was limited by using comparable exposure times (400–500 ms) in all non-DAPI filters. This was particularly relevant for the Cy5 filter where three different spectra were being deconvoluted. Specificity and correct separation of spectra was assessed by comparison to single marker patterns (Supplementary material, Figure S2). Autofluorescence of erythrocytes in FFPE material is a notorious issue for the evaluation of IF signals. Erythrocytes, however, were morphologically distinct from cells of interest and lacked expression of membrane markers. We addressed this issue through extensive training and segmentation with the InForm software, enabling the system to differentiate between cells of interest and erythrocytes.

After optimisation, all markers could be discriminated in the tumour tissues. Immune cell populations defined as $CD3^+CD8^-$ T-cells (mostly T-helper cells), cytotoxic T-cells ($CD3^+CD8^+$), regulatory T-cells ($CD3^+FOXP3^+$), memory T-cells ($CD3^+CD45RO^+$), and activated, cytotoxic T-cells ($CD3^+GZMB^+$) could be successfully identified and counted using the InForm software (Supplementary material, Figure S3). Furthermore, phenotype counts were compared between seven-marker and single-marker detection in consecutive tissue sections of a MMR-deficient (MMR-D) and MMR-proficient MMR-P CRC, to exclude biases introduced by the combination of antibodies and separation of spectra (Supplementary material, Table S1). After this, the T-cell panel was applied for the characterisation of 19 colorectal cancer tissues, of which four were MMR-D. Using the approach

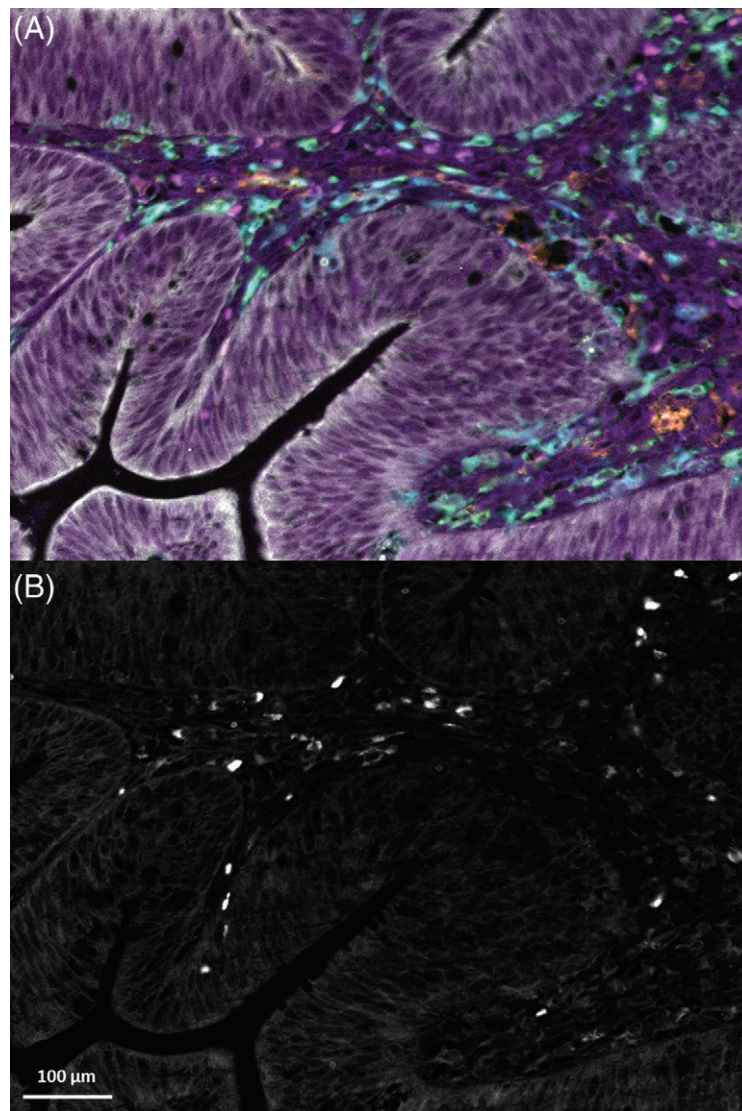


Figure 4. (A) Immunofluorescent detection of myeloid-related markers in colorectal cancer tissue in which PD-L1 was enhanced by TSA. Markers are PD-L1 (magenta), HLA-DR (orange), CD11c (blue), CD163 (green), CD68 (cyan), and keratin (white). (B) TSA-enhanced PD-L1 only, in the same tissue.

described here it was possible to phenotype and count the different T-cell phenotypes at various cellular densities across the tissues (Figure 3). Furthermore, the T-cell phenotypes were compared between MMR-D and MMR-P tumours which showed distinctly higher cytotoxic and memory T-cell densities in MMR-D tumours (Figure 3).

TSA can be specifically employed for the detection of low abundance antigens in combination with direct and indirect IF

For the detection of antigens with low expression level, fluorescence signal amplification might be

desirable. Therefore, we assessed if our methodology was compatible with applying TSA for selected markers. Here, we assessed the expression of PD-L1, CD11c, HLA-DR, CD163, keratin, and CD68 (myeloid panel) in a colorectal cancer tissue. PD-L1 detection was challenging with both direct and indirect IF and therefore TSA with Opal 520 was applied to assess the expression of this molecule. Figure 4 demonstrates the successful detection of PD-L1 together with six other markers detected by indirect and direct IF. Thus, we show that TSA detection can be easily combined with the current method for the detection of low abundance proteins without requiring subsequent steps of TSA-based detection.

Discussion

The increasing amount of data highlighting the importance of cancer immunophenotypes in predicting patient prognosis and response to immunotherapies underlines the need for high-throughput immunophenotyping tools that can be easily applied in a clinical context. Here, we describe an efficient and fast seven-colour IF method for the analysis of tumour tissues by multispectral microscopy. The use of primary antibodies that are detected with fluorescent secondary antibodies, followed by the detection of antigens by directly conjugated antibodies, allows the use of two or more antibodies of the same isotype in one sample. The limitations of standardising exposure times and spectral overlap in different or the same optical filters can be easily overcome. Moreover, this method is time-efficient when compared to the consecutive detection of single antigens, which is currently applied in other multiplex immunodetection techniques. Furthermore, the challenges in evaluating the expression of low expressed antigens can be addressed by combining the current method with TSA-based antigen detection.

Efficient multiplex IF detection methods are becoming essential in the assessment of immune cell infiltration, which can have large implications for patient prognosis. For instance, targeting the PD-L1/PD1 axis has shown great applicability for the treatment of tumours with high mutation burden [5,6,8]. Nevertheless, not all patients respond to checkpoint blockade and this differential sensitivity to treatment might be explained by the immune cell composition of the tumour microenvironment [25,26]. Besides aiding patient selection for current (immuno-) therapies, multiplex immunophenotyping can lead to the identification of distinct immunophenotypes that pose potential targets for immunotherapy [27]. In this work we describe two panels that can be readily applied for the detection of lymphoid and myeloid immune cells.

High cytotoxic T-cell densities have been associated with a better prognosis in solid cancers [9–12] while the presence of regulatory T-cells has been associated with improved clinical outcome when cells reside inside the tumour tissue but with a worse prognosis when present in the tumour surroundings [28,29]. Importantly, the ratio between cytotoxic T-cells and regulatory T-cells appears to be particularly relevant for patient prognosis [30,31]. Furthermore, increased infiltration of memory T-cells (CD45RO⁺) in tumours has also been associated with a favourable clinical outcome [11,32]. All these parameters can be readily investigated in retrospective cohorts with the T-cell panel described here.

The current myeloid panel was conceptualised to test the combination of the TSA method with indirect and direct IF. Tumour-associated macrophages (TAMs) play an important role in cancer pathogenesis [33]. In several cancer types, the polarisation between classically (M1) and alternatively (M2) activated macrophages is thought to be crucial for disease progression [34,35]. Our myeloid panel is able to discern M1 (CD68⁺HLA-DR⁺) and M2 (CD68⁺CD163⁺PD-L1⁺) related phenotypes in cancer tissues as well as to assess tumour infiltration by dendritic cells (CD11c⁺).

In conclusion, we have developed a method for IF detection of seven markers in FFPE tissue that can be directly applied for extensive immunophenotyping. The method is time-efficient because it does not involve the use of TSA-based detection protocols which also prevents tissue damage as a consequence of repeated boiling or bleaching for antibody stripping. This technique may serve as a diagnostic tool and is also highly complementary to techniques such as (single cell) RNA sequencing or mass cytometry that require validation in extensive cohorts of archival tissue.

Acknowledgements

This work was supported by the Fight Colorectal Cancer-Michael's Mission-AACR Fellowship (2015), Alpe d'HuZes/KWF Bas Mulder Award (UL2015-7664), Veni ZonMw grant (91617144), and the European Commission H2020 MSCA-ETN grant under proposal number 675743 (project acronym: ISPIC).

Author contributions statement

MEIJ, TPB, and NFM planned experiments, analysed data, and wrote the manuscript. MEIJ, TPB, ZA, ER, AR, and AMH conducted experiments; AV, ESJ, and NFM supervised all immunofluorescent experiments. NFM designed and directed the project. All authors contributed to and had final approval of the submitted manuscript.

References

1. Brahmer JR, Tykodi SS, Chow LQ, *et al.* Safety and activity of anti-PD-L1 antibody in patients with advanced cancer. *N Engl J Med* 2012; **366**: 2455–2465.
2. Hodi FS, O'Day SJ, McDermott DF, *et al.* Improved survival with ipilimumab in patients with metastatic melanoma. *N Engl J Med* 2010; **363**: 711–723.

3. Le DT, Uram JN, Wang H, et al. PD-1 blockade in tumors with mismatch-repair deficiency. *N Engl J Med* 2015; **372**: 2509–2520.
4. Topalian SL, Hodi FS, Brahmer JR, et al. Safety, activity, and immune correlates of anti-PD-1 antibody in cancer. *N Engl J Med* 2012; **366**: 2443–2454.
5. Gibney GT, Weiner LM, Atkins MB. Predictive biomarkers for checkpoint inhibitor-based immunotherapy. *Lancet Oncol* 2016; **17**: e542–e551.
6. Le DT, Durham JN, Smith KN, et al. Mismatch repair deficiency predicts response of solid tumors to PD-1 blockade. *Science* 2017; **357**: 409–413.
7. Riaz N, Havel JJ, Makarov V, et al. Tumor and microenvironment evolution during immunotherapy with Nivolumab. *Cell* 2017; **171**: 934–949 e915.
8. Rizvi NA, Hellmann MD, Snyder A, et al. Cancer immunology. Mutational landscape determines sensitivity to PD-1 blockade in non-small cell lung cancer. *Science* 2015; **348**: 124–128.
9. de Miranda NF, Goudkade D, Jordanova ES, et al. Infiltration of lynch colorectal cancers by activated immune cells associates with early staging of the primary tumor and absence of lymph node metastases. *Clin Cancer Res* 2012; **18**: 1237–1245.
10. Fridman WH, Pages F, Sautes-Fridman C, et al. The immune contexture in human tumours: impact on clinical outcome. *Nat Rev Cancer* 2012; **12**: 298–306.
11. Galon J, Costes A, Sanchez-Cabo F, et al. Type, density, and location of immune cells within human colorectal tumors predict clinical outcome. *Science* 2006; **313**: 1960–1964.
12. Punt S, Dronkers EA, Welters MJ, et al. A beneficial tumor microenvironment in oropharyngeal squamous cell carcinoma is characterized by a high T cell and low IL-17(+) cell frequency. *Cancer Immunol Immunother* 2016; **65**: 393–403.
13. Martens A, Wistuba-Hamprecht K, Geukes Foppen M, et al. Baseline peripheral blood biomarkers associated with clinical outcome of advanced melanoma patients treated with ipilimumab. *Clin Cancer Res* 2016; **22**: 2908–2918.
14. van Dongen JJ, Lhermitte L, Bottcher S, et al. EuroFlow antibody panels for standardized n-dimensional flow cytometric immunophenotyping of normal, reactive and malignant leukocytes. *Leukemia* 2012; **26**: 1908–1975.
15. Yuan J, Hegde PS, Clynes R, et al. Novel technologies and emerging biomarkers for personalized cancer immunotherapy. *J Immunother Cancer* 2016; **4**: 3.
16. van Unen V, Li N, Molendijk I, et al. Mass cytometry of the human mucosal immune system identifies tissue- and disease-associated immune subsets. *Immunity* 2016; **44**: 1227–1239.
17. Angelova M, Charoentong P, Hackl H, et al. Characterization of the immunophenotypes and antigenomes of colorectal cancers reveals distinct tumor escape mechanisms and novel targets for immunotherapy. *Genome Biol* 2015; **16**: 64.
18. Bendall SC, Nolan GP, Roederer M, et al. A deep profiler's guide to cytometry. *Trends Immunol* 2012; **33**: 323–332.
19. Tsujikawa T, Kumar S, Borkar RN, et al. Quantitative multiplex immunohistochemistry reveals myeloid-inflamed tumor-immune complexity associated with poor prognosis. *Cell Rep* 2017; **19**: 203–217.
20. Glass G, Papin JA, Mandell JW. SIMPLE: a sequential immunoperoxidase labeling and erasing method. *J Histochem Cytochem* 2009; **57**: 899–905.
21. Parra ER, Uraoka N, Jiang M, et al. Validation of multiplex immunofluorescence panels using multispectral microscopy for immune-profiling of formalin-fixed and paraffin-embedded human tumor tissues. *Sci Rep* 2017; **7**: 13380.
22. Toth ZE, Mezey E. Simultaneous visualization of multiple antigens with tyramide signal amplification using antibodies from the same species. *J Histochem Cytochem* 2007; **55**: 545–554.
23. Huang W, Hennrick K, Drew S. A colorful future of quantitative pathology: validation of Vectra technology using chromogenic multiplexed immunohistochemistry and prostate tissue microarrays. *Hum Pathol* 2013; **44**: 29–38.
24. Hall G, Clarkson A, Shi A, et al. Immunohistochemistry for PMS2 and MSH6 alone can replace a four antibody panel for mismatch repair deficiency screening in colorectal adenocarcinoma. *Pathology* 2010; **42**: 409–413.
25. Hegde PS, Karanikas V, Evers S. The where, the when, and the how of immune monitoring for cancer immunotherapies in the era of checkpoint inhibition. *Clin Cancer Res* 2016; **22**: 1865–1874.
26. Wei SC, Levine JH, Cogdill AP, et al. Distinct cellular mechanisms underlie anti-CTLA-4 and anti-PD-1 checkpoint blockade. *Cell* 2017; **170**: 1120–1133, e1117.
27. Whiteside TL, Demaria S, Rodriguez-Ruiz ME, et al. Emerging opportunities and challenges in cancer immunotherapy. *Clin Cancer Res* 2016; **22**: 1845–1855.
28. Saito T, Nishikawa H, Wada H, et al. Two FOXP3(+)/CD4(+) T cell subpopulations distinctly control the prognosis of colorectal cancers. *Nat Med* 2016; **22**: 679–684.
29. Salama P, Phillips M, Grieco F, et al. Tumor-infiltrating FOXP3(+) T regulatory cells show strong prognostic significance in colorectal cancer. *J Clin Oncol* 2009; **27**: 186–192.
30. Jordanova ES, Gorter A, Ayachi O, et al. Human leukocyte antigen class I, MHC class I chain-related molecule A, and CD8+/regulatory T-cell ratio: which variable determines survival of cervical cancer patients? *Clin Cancer Res* 2008; **14**: 2028–2035.
31. Suzuki H, Chikazawa N, Tasaka T, et al. Intratumoral CD8(+) T/FOXP3(+) cell ratio is a predictive marker for survival in patients with colorectal cancer. *Cancer Immunol Immun* 2010; **59**: 653–661.
32. Hu GM, Wang SM. Tumor-infiltrating CD45RO(+) memory T lymphocytes predict favorable clinical outcome in solid tumors. *Sci Rep* 2017; **7**: 10376.
33. Engblom C, Pfirschke C, Pittet MJ. The role of myeloid cells in cancer therapies. *Nat Rev Cancer* 2016; **16**: 447–462.
34. Kurahara H, Shintani H, Mataka Y, et al. Significance of M2-polarized tumor-associated macrophage in pancreatic cancer. *J Surg Res* 2011; **167**: E211–E219.
35. Yuan A, Hsiao YJ, Chen HY, et al. Opposite effects of M1 and M2 macrophage subtypes on lung cancer progression. *Sci Rep* 2015; **5**: 14273.

SUPPLEMENTARY MATERIAL ONLINE

Figure S1. Workflow for image analysis by the InForm software

Figure S2. Single marker immunofluorescent detection of T-cell markers in tonsil tissue

Figure S3. Detection of immunophenotypes in tumour tissue by the InForm software

Table S1. Comparison of phenotype counts between seven-marker labelled and single-marker labelled consecutive tissue sections